BUTTERWORTH HEINEMANN

Polymer Vol. 36 No. 12, pp. 2451–2462, 1995
Elsevier Science Ltd
Printed in Great Britain

Effect of flow geometry on the rheology of dispersed two-phase blends of polystyrene and poly(methyl methacrylate)

James H. Han, Chin Choi-Feng and De-Jie Li
Research and Development, Amoco Polymer Group, Naperville, IL 60566, USA

and Chang Dae Han*
Department of Polymer Engineering, The University of Akron, Akron, OH 44325, USA
(Received 5 October 1994)

The rheological properties of blends of poly(methyl methacrylate) (PMMA) and polystyrene (PS), forming two phases in the molten state, were measured using cone-and-plate and capillary rheometers. For the PS/PMMA blends, we have found that logarithmic plots of steady shear viscosity *versus* shear rate obtained by a cone-and-plate rheometer do not overlap those obtained by a capillary rheometer, whereas for the homopolymers PS and PMMA there is a good agreement between the two. This observation is explained in terms of the differences in the morphological states of the blends between the uniform shear flow in a cone-and-plate rheometer and the non-uniform shear flow in a capillary rheometer, which involves the entrance and exit effects. We have pointed out that, owing to the changes occurring in the shape of the dispersed droplets in the entrance region of a cylindrical die, the use of the Bagley plot to calculate shear stresses (thus shear viscosities) of dispersed two-phase polymer blends is of no rheological significance. We have also pointed out that the Cox–Merz rule does not hold for dispersed two-phase polymer blends, because the morphology of a dispersed two-phase blend in oscillatory shear flow would not be the same as that in steady shear flow. We have found that in the terminal region, logarithmic plots of dynamic storage modulus (G') *versus* dynamic loss modulus (G'') give rise to curvature for the PS/PMMA blends but a straight line for the constituent components, leading us to conclude that such plots are very sensitive to variations in the morphological state of the blends.

(Keywords: two-phase blends; flow geometry; rheology)

INTRODUCTION

The rheological behaviour of multiphase polymer systems, including incompatible (i.e. two-phase) polymer blends, is intimately related to their morphology[1,2]. Specifically, the importance of rheology–morphology relationships in two-phase polymer blends was emphasized in the 1970s in a series of papers by Han and co-workers[3–8], van Oene[9] and Vinogradov and co-workers[10]. In the 1980s other research groups[11,12] studied the same subject.

In investigating the rheological behaviour of molten polymers, it is customary to use a cone-and-plate rheometer at low shear rates, and a capillary (or slit) rheometer at high shear rates. There are two methods for determining the wall shear stress (thus shear viscosity) using a cylindrical (or slit) die[13]: (a) to measure the total pressure drop from a point in the upstream of the reservoir to the die exit and then calculate wall shear stresses (thus shear viscosities) by making use of the Bagley plot for end corrections; and (b) to measure wall normal stresses along the die axis and then calculate wall shear stresses (thus shear viscosities) using the constancy of pressure gradient, $-\partial p/\partial z$. In the first method, the end correction can be neglected for all intents and purposes when a sufficiently long die is used; in the second method, pressure transducers must be mounted on the die wall at distances sufficiently far from the entrance region, such that a constancy of $-\partial p/\partial z$ can be established. There is ample experimental evidence in the literature[1,2] that for single-phase (i.e. homogeneous) polymer melts, plots of shear viscosity *versus* shear rate obtained from a cone-and-plate rheometer overlap those obtained from a capillary (or slit) rheometer. However, the same situation may not hold for two-phase polymer blends (and multiphase polymeric systems in general).

In investigating the rheological behaviour of two-phase polymer blends, Han and co-workers[3–8] measured wall normal stresses along the axis of a slit or cylindrical die and used constancy of $-\partial p/\partial z$ in the downstream direction of the die to calculate wall shear stresses and thus apparent bulk shear viscosities. As pointed out by Han and Charles[14], the constancy of $-\partial p/\partial z$ meets with necessary and sufficient conditions for Newtonian fluids to be fully developed, but it only meets with a necessary condition for viscoelastic fluids to be fully developed. In the flow of a dispersed two-phase polymer blend through a slit (or cylindrical) die, it is not difficult

*To whom correspondence should be addressed

to envisage that the shape of the droplets may change in the entrance region[15]. It can be surmised that dispersed two-phase polymer blends will require a longer die to achieve a constancy of $-\partial p/\partial z$ than single-phase (homogeneous) polymers. In the absence of direct visual observations as to how the shape of droplets changes inside a die, one may assume that a dispersed two-phase polymer blend has attained fully developed flow in a slit (or cylindrical) die when a constancy of $-\partial p/\partial z$ is attained. In other words, the constance of $-\partial p/\partial z$ meets at least with the necessary condition for fully developed flow of dispersed two-phase polymer blends.

Very recently, we measured the rheological properties of two-phase blends of polystyrene and poly(methyl methacrylate) using a cone-and-plate rheometer at low shear rates and a capillary rheometer at high shear rates. For the capillary rheometer, we measured the total pressure drop from a point in the upstream of the reservoir to the die exit for a given flow rate. Samples were collected after rheological measurements from the cone-and-plate and capillary rheometers, respectively, and micrographs of the samples were taken using transmission electron microscopy.

The purpose of this paper is to show that (a) in dealing with two-phase polymer blends, plots of shear viscosity *versus* shear rate (or shear stress) obtained from a cone-and-plate rheometer do not necessarily overlap those obtained from a capillary (or slit) rheometer, and (b) the assumptions implied in the Bagley plot, which has proved useful for homogeneous polymer melts, are not valid for two-phase polymer blends, and the calculation of wall shear stress (thus shear viscosities) using the measurements of the total pressure drop from a point upstream of the reservoir to the die exit gives rise to inaccurate information. Using the micrographs of the samples collected from each experimental run, we explain the differences observed between the plots of shear viscocity *versus* shear stress obtained from a cone-and-plate rheometer and similar plots obtained from a capillary rheometer.

EXPERIMENTAL

Materials

Commercial grades of polystyrene (PS) (Dow Chemical, STYRON 685D) and poly(methyl methacrylate) (PMMA) (Rohm and Haas, Plexiglas V920) were used to prepare binary blends in a twin-screw compounding machine (Werner and Pfleiderer, ZDSK-53). The mixing of the materials was achieved by conveying and kneading with screw bushings and kneading elements assembled along the screw. The material was discharged through a die plate and into a water bath. The strands quenched in the water bath were then cut into pellets. The blend ratios prepared were PMMA/PS 90/10, 70/30, 50/50, 30/70 and 10/90, where the number denotes the weight percentage.

Rheological measurements

The Rheometrics Dynamic Analyzer (model RDA II) was used to measure the steady shear viscosity η as a function of shear rate $\dot{\gamma}$ (or shear stress σ), and the oscillatory shear flow properties (dynamic storage modulus G' and dynamic loss modulus G'') as a function of angular frequency ω. Using the values of G' and G'', the complex viscosity $|\eta^*|$ was calculated from the expression $|\eta^*(\omega)| = [(G'(\omega)/\omega)^2 + (G''(\omega)/\omega)^2]^{1/2}$. For the viscosity measurements at high shear rates a Goettfert capillary rheometer (model 2002) was employed, using capillaries with varying length-to-diameter ratios: $L/D = 30$, 40 and 60, where $D = 0.1$ cm.

Microscopy

A transmission electron microscope (Philips 400 T) was used to examine the phase morphology of the binary blend specimens before and/or after the shear flow experiment. Ultrathin sections of the blend specimens were obtained by ultramicrotome and coated lightly with carbon in a vacuum evaporator.

RESULTS AND DISCUSSION

Effect of flow geometry on the steady shear viscosity of PMMA/PS blends

Figure 1 gives plots of $\log \eta$ *versus* $\log \dot{\gamma}$ for PS at 210, 220 and 230°C, where filled symbols represent the data obtained with the cone-and-plate rheometer and open symbols represent the data obtained with the capillary rheometer. It should be mentioned that in the analysis of the capillary data presented in *Figure 1*, $\dot{\gamma}$ denotes the true shear rate with the Rabinowitch–Mooney correction. It can be seen in *Figure 1* that the cone-and-plate data overlap very well with the capillary data. Note that the end correction was neglected in the analysis of the capillary die data, which were taken using $L/D = 30$. *Figure 1* seems to indicate that, for all intents and purposes, the neglect of end corrections for the PS in the analysis of the capillary data based on $L/D = 30$ is acceptable.

For the reason that shear rate is ill-defined in the analysis of the rheological data for PMMA/PS blends (and for multiphase fluid systems in general) because the velocity gradient is not continuous at the phase interface between the components[1,2], we prepared plots of $\log \eta$ *versus* $\log \sigma$ at 210, 220 and 230°C for PS, and they are given in *Figure 2*. Here we assume that the shear stress is continuous at the phase interface, which seems reasonable in most situations. Again, the cone-and-plate data overlap very well the capillary data.

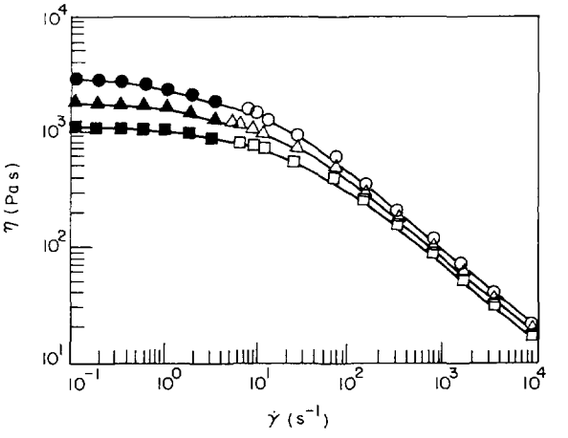

Figure 1 Plots of $\log \eta$ *versus* $\log \dot{\gamma}$ for homopolymer PS at: (●, ○) 210 C; (▲, △) 220 C; (■, □) 230 C, where filled symbols denote cone-and-plate data and open symbols denote capillary data

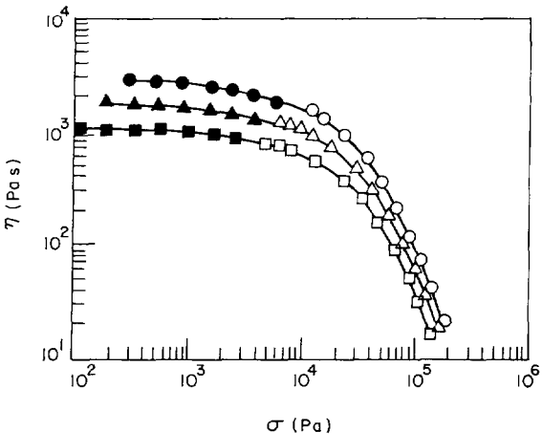

Figure 2 Plots of $\log \eta$ *versus* $\log \sigma$ for homopolymer PS at: (●, ○) 210 C; (▲, △) 220 C; (■, □) 230 C, where filled symbols denote cone-and-plate data and open symbols denote capillary data

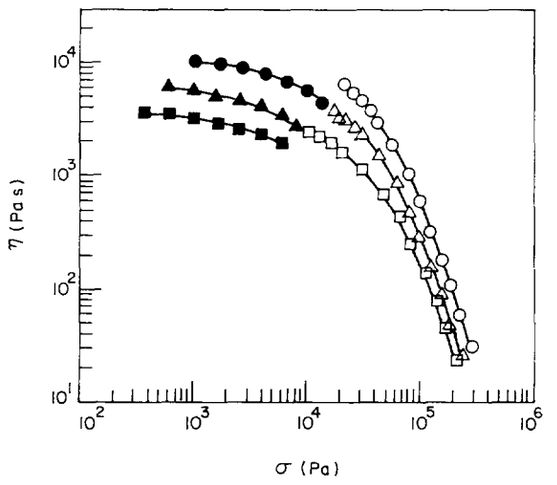

Figure 3 Plots of $\log \eta$ *versus* $\log \sigma$ for the 90/10 PMMA/PS blend at: (●, ○) 210 C; (▲, △) 220 C; (■, □) 230 C, where filled symbols denote cone-and-plate data and open symbols denote capillary data

Figure 3 gives plots of $\log \eta$ *versus* $\log \sigma$ for the 90/10 PMMA/PS blend at 210, 220 and 230°C, where filled symbols represent the data obtained with the cone-and-plate rheometer and open symbols represent the data obtained with the capillary rheometer. It can be seen in *Figure 3* that there is no overlap between cone-and-plate data and capillary data; namely, the capillary data show much higher visocity than the cone-and-plate data. We observe the same trend in the other blend compositions: *Figure 4* for the 70/30 PMMA/PS blend at 210, 220 and 230°C; *Figure 5* for the 50/50 PMMA/PS blend at 210, 220 and 230°C; *Figure 6* for the 30/70 PMMA/PS blend at 210, 220 and 230°C; and *Figure 7* for the 10/90 PMMA/PS blend at 210, 220 and 230°C. Before proceeding further, we will describe the procedures used to calculate the values of η, presented in *Figures 3–7*, using the capillary data.

In dealing with homogeneous fluids flowing through a long cylindrical die, the viscosity η can be determined from the expression:

$$\eta = \sigma/\dot{\gamma} \tag{1}$$

where σ is the shear stress at the tube wall and $\dot{\gamma}$ is the

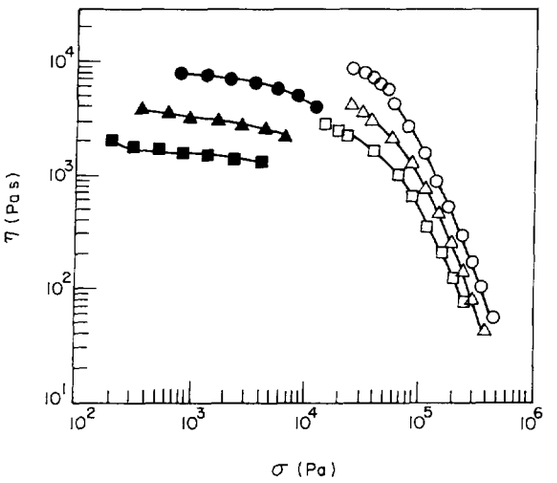

Figure 4 Plots of $\log \eta$ *versus* $\log \sigma$ for the 70/30 PMMA/PS blend at: (●, ○) 210 C; (▲, △) 220 C; (■, □) 230 C, where filled symbols denote cone-and-plate data and open symbols denote capillary data

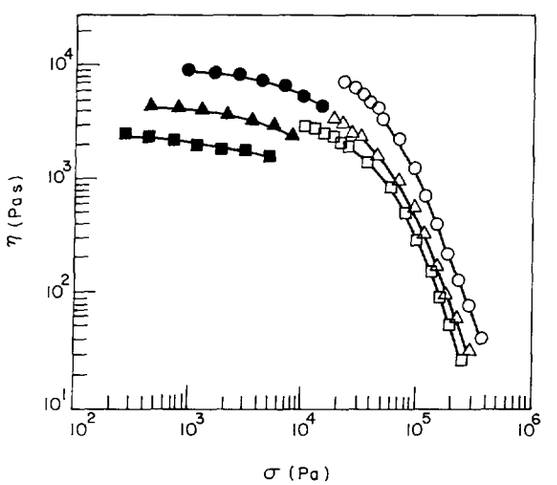

Figure 5 Plots of $\log \eta$ *versus* $\log \sigma$ for the 50/50 PMMA/PS blend at: (●, ○) 210 C; (▲, △) 220 C; (■, □) 230 C, where filled symbols denote cone-and-plate data and open symbols denote capillary data

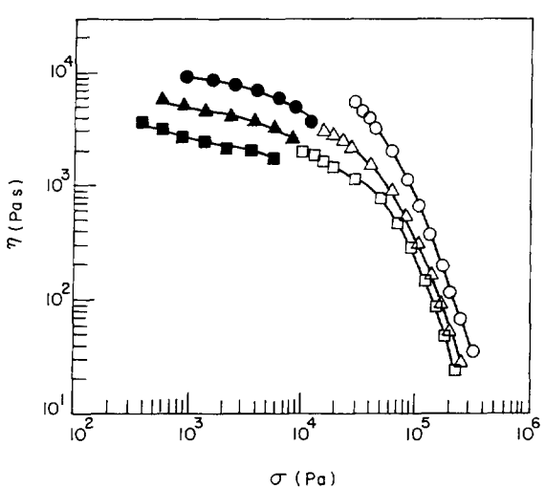

Figure 6 Plots of $\log \eta$ *versus* $\log \sigma$ for the 30/70 PMMA/PS blend at: (●, ○) 210 C; (▲, △) 220 C; (■, □) 230 C, where filled symbols denote cone-and-plate data and open symbols denote capillary data

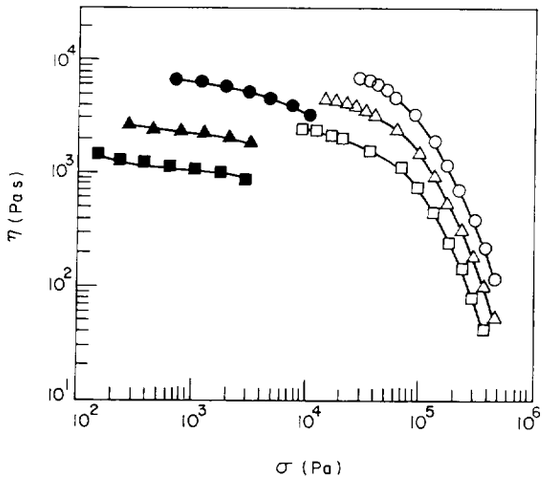

Figure 7 Plots of $\log \eta$ *versus* $\log \sigma$ for the 10/90 PMMA/PS blend at: (●, ○) 210 C; (▲, △) 220 C; (■, □) 230 C, where filled symbols denote cone-and-plate data and open symbols denote capillary data

shear rate. Note that σ can be calculated from[13]:

$$\sigma = (-\partial p/\partial z)D/4 \tag{2}$$

where $-\partial p/\partial z$ is the axial pressure gradient in the fully developed region and D is the tube diameter. Experimental determination of $-\partial p/\partial z$ (thus σ) can be made easily when wall normal stresses at the die wall are measured in the fully developed region of the die[13]. However, as is the case in the present study, very often one only measures the pressure at a point in the upstream of the reservoir and calculates σ using the following expression[13]:

$$\sigma = \frac{\Delta P}{4(L/D + n_{end})} \tag{3}$$

where ΔP is the total pressure drop from a point in the upstream of the reservoir to the die exit, and n_{end} is the end correction necessary for short dies, which is usually obtained from the Bagley plot. In order to obtain the true values of viscosity from the capillary data, one must make the so-called Rabinowitch–Mooney correction for shear rate $\dot{\gamma}$:

$$\dot{\gamma} = \frac{\dot{\gamma}_{app}}{4}\left(3 + \frac{\mathrm{d} \ln \dot{\gamma}_{app}}{\mathrm{d} \ln \sigma}\right) \tag{4}$$

where $\dot{\gamma}_{app}$ denotes the apparent shear rate defined by:

$$\dot{\gamma}_{app} = 32Q/\pi D^3 \tag{5}$$

in which Q is the volumetric flow rate and D is the capillary diameter.

When dealing with dispersed two-phase polymer blends, one encounters a dilemma with calculating σ using equation (3), because the deformation of the discrete phase (i.e. droplets) in the entrance region and/or droplet break-up in the stress relaxation region, as demonstrated clearly by Chin and Han[15,16], make the assumptions made in the Bagley plot untenable, i.e. the use of the Bagley plot is valid only for homogeneous fluids. It should be mentioned that, for all intents and purposes, for a sufficiently long die the term n_{end} appearing in equation (3) can be neglected. However, this simplification does not alleviate the dilemma described above in the use of equation (3) for dispersed two-phase polymer blends. In this regard, when dealing with dispersed two-phase polymer blends, the use of equation (2) is most desirable to determine the value of σ, provided that the state of dispersion (i.e. the shape of the dispersed droplets) remains constant in the region where $-\partial p/\partial z$ is constant downstream of the capillary. In their studies on the rheological behaviour of two-phase polymer blends, Han and co-workers[3–8] measured pressure profiles in the fully developed region and thus used equation (2).

In calculating the values of η from the capillary data given in *Figures 3–7*, we used equation (3) to calculate σ by neglecting the term n_{end}. Even for a sufficiently long die, strictly speaking this approach is not valid because equation (3) is valid only for homogeneous fluids. Moreover, there is an additional dilemma in calculating from equation (1) the values of η for dispersed two-phase polymer blends, because equation (4) was derived with the assumption that the velocity gradient in the fluid is continuous across the diameter of the cylindrical tube[1,3], which certainly is not true for dispersed two-phase polymer blends. It should be mentioned that the velocity gradient is discontinuous at the phase interface when the viscosities of the two fluids are different[1,2]. Therefore the use of equation (4) to calculate $\dot{\gamma}$ is not valid for dispersed two-phase polymer blends. Perhaps, a more prudent approach might be to use the apparent shear rate $\dot{\gamma}_{app}$ defined by equation (5), and then calculate apparent bulk shear viscosity η_{app} defined by:

$$\eta_{app} = \sigma/\dot{\gamma}_{app} \tag{6}$$

Thus the lack of overlap in the plots of $\log \eta$ *versus* $\log \sigma$ between the cone-and-plate data and the capillary data, displayed in *Figures 3–7*, is attributable to the fact that the morphology of a PMMA/PS blend subjected to the shear flow field in the cone-and-plate rheometer was not the same as the morphology of the blend subjected to the shear flow field in the capillary rheometer. This will be demonstrated below when presenting the micrographs of the specimens, which were subjected to flow either in a cone-and-plate rheometer or in a capillary rheometer. For now, in order to facilitate our discussion here, let us look at *Figure 8a*, which describes schematically the shape of droplets in a uniform shear flow field, and *Figure 8b*, which describes schematically the shape of droplets in a non-uniform shear flow field. In *Figure 8b* we consider the fully developed region in the capillary die, where the shape of the droplets remains constant along the flow direction.

It is clear from *Figure 8* that in a uniform shear flow field (i.e. in the cone-and-plate rheometer) the shape of droplets would be the same at various positions along the y-axis, whereas in a non-uniform shear flow field (i.e. in the capillary die) the shape of droplets would be different at various positions along the r-axis. Thus, we can surmise that, owing to the different shapes of droplets that might be present in the two shear flow fields, the rheological properties of a dispersed two-phase polymer blend determined with a capillary rheometer would be different from those determined with a cone-and-plate rheometer. This can now explain why in *Figures 3–7* there is no overlap in the shear viscosities of the PMMA/PS blends between cone-and-plate data and capillary data. Note that in *Figure 2* there is a very good overlap in the

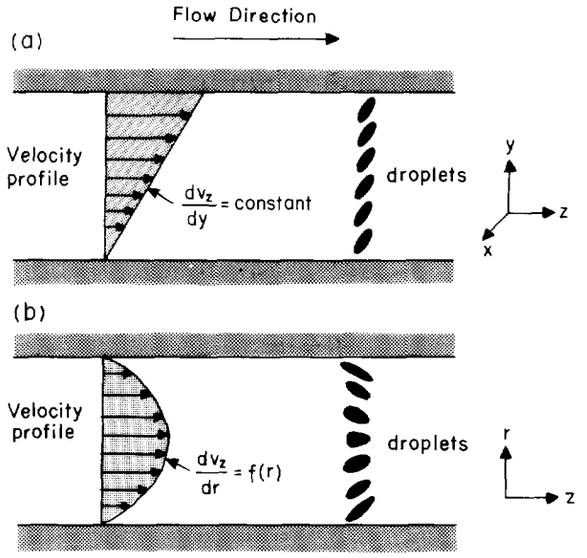

Figure 8 Schematic diagrams describing the velocity profiles and droplet shapes (a) in a uniform shear flow field and (b) in a non-uniform shear flow field

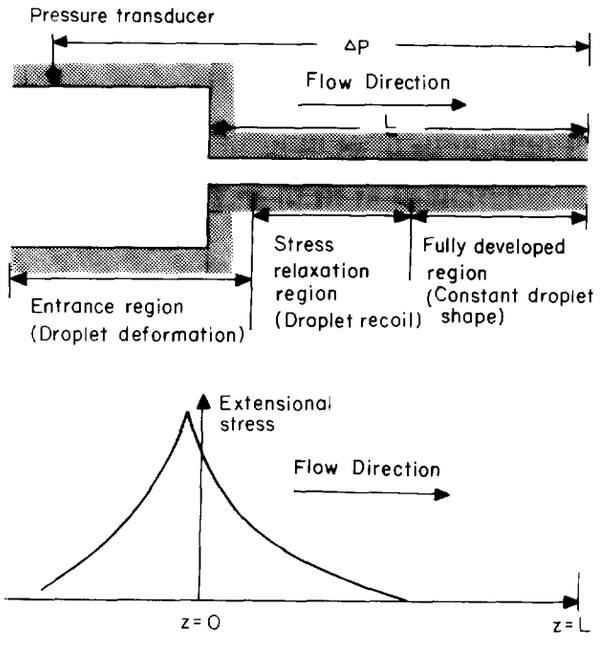

Figure 9 The upper panel describes schematically (i) the entrance region where droplet deformation occurs, (ii) the stress relaxation region where the elongated droplet may recoil or break up, and (iii) the fully developed region where the droplet shape remains constant in the cylindrical tube. The lower panel describes schematically the extensional stress distribution in a cylindrical tube along the flow direction

shear viscosities of homopolymer PS between cone-and-plate data and capillary data.

In order to better understand the mechanisms of droplet deformation and break-up in a non-uniform shear flow field, let us look at a schematic, given in the upper panel of *Figure 9*, describing various regions in a cylindrical die, namely (a) the entrance region where droplet deformation may occur, (b) the stress relaxation region where droplet recoil may occur, and (c) the fully developed region where the droplet shape remains constant. The lower panel of *Figure 9* shows a schematic describing the stress distribution along the centre-line of the die, following the studies of Vinogradov and co-workers[17] and Yoo and Han[18]. Thus, the droplets in the entrance region may be elongated; a droplet is elongated by the acceleration of the velocity (or stress build-up) in the entrance region and then recoils, upon passing the entrance region, owing to the deceleration of the velocity (or stress relaxation) until the flow becomes fully developed. Note that the shape of the droplet will remain constant in the fully developed region of the die. It is not difficult to imagine that in real situations, where a two-phase PMMA/PS blend flows through a cylindrical die, there are many droplets of varying sizes, making the analysis of flow very complicated. Further details of the mechanism(s) of droplet break-up in a non-uniform shear flow may be found in refs 16 and 19.

On the basis of the observations made above, we can conclude that there is no *a priori* reason why one should expect to observe an overlap in the rheological properties of two-phase polymer blends between cone-and-plate data and capillary data. This conclusion is also applicable to other multiphase polymer systems, such as microphase-separated block copolymers and liquid-crystalline polymers. As a matter of fact, very recently Han and co-workers[20] have demonstrated that there was no overlap in the shear viscosities of microphase-separated styrene-based triblock copolymers between cone-and-plate data and capillary data.

The morphology of PMMA/PS blends

Micrographs were taken of the PMMA/PS blend samples, which were subjected either to a uniform shear flow field (i.e. in a cone-and-plate rheometer) or to a non-uniform shear flow field (i.e. in a capillary rheometer). *Figures 10–13* show some repesentative micrographs which will help to interpret the rheological data presented above. It should be mentioned that all the micrographs were taken using specimens that were rapidly quenched after being sheared either in a cone-and-plate rheometer at $\dot{\gamma} = 0.1$ or $1\ s^{-1}$, or in a capillary rheometer at $\dot{\gamma} = 10$ or $100\ s^{-1}$.

Figure 10 gives micrographs for the 90/10 PMMA/PS blend, in which the dark area represents the PS phase and the white area represents the PMMA phase, before and after being subjected to shear flow at 210°C. The following observations are worth noting in *Figure 10*. (1) When a specimen was subjected to steady shear flow in the cone-and-plate rheometer at a shear rate as low as $0.1\ s^{-1}$, break-up of the dispersed PS droplets occurred, giving rise to sizes which are much smaller than those prior to the applied shear flow (compare *Figure 10b* with *Figure 10a*). (2) The dispersed PS droplets elongated along the flow direction. (3) Long thread-like droplets with non-uniform diameter together with almost spherical droplets of small sizes coexist in the specimens when subjected to shear flow in the cone-and-plate rheometer at $\dot{\gamma} = 1\ s^{-1}$ or in the capillary rheometer at $\dot{\gamma} = 10\ s^{-1}$, as can be seen in *Figures 10c* and *10d*.

Figure 11 gives micrographs for the 70/30 PMMA/PS blend before and after being subjected to shear flow at 210°C. The following observations are worth noting in *Figure 11*. (1) In the blend prepared with a twin-screw extruder, there are both large and small droplets in this blend (see *Figure 11a*). The droplets of small sizes must

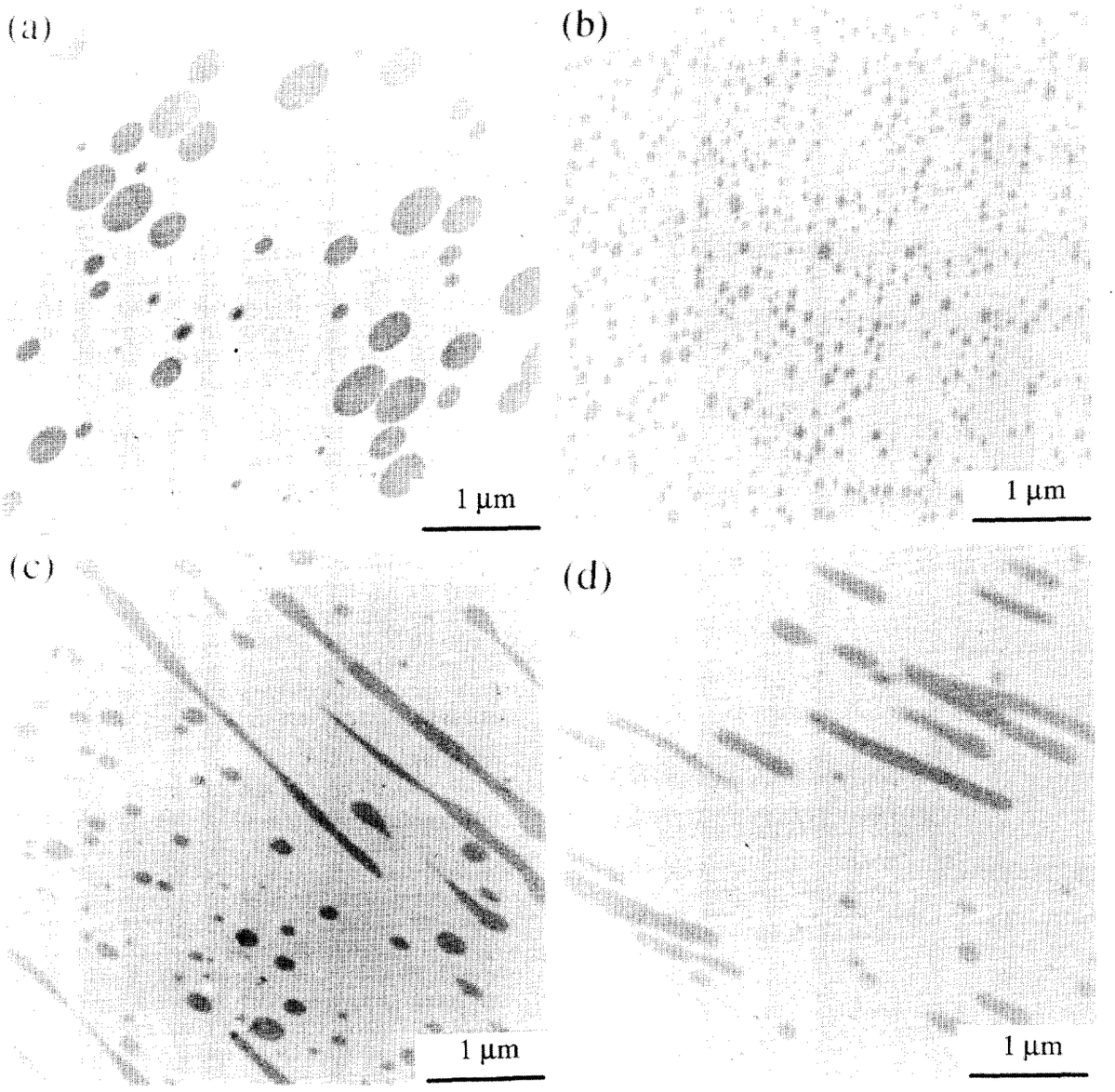

Figure 10 Micrographs for the 90/10 PMMA/PS blend, in which the dark area represents the PS phase and the white area represents the PMMA phase: (a) before being subjected to shear flow; (b) the cross-section of the specimen after being subjected to shear flow at $\dot{\gamma} = 1\,s^{-1}$; (c) along the flow direction after being subjected to shear flow at $\dot{\gamma} = 1\,s^{-1}$; (d) along the flow direction after being subjected to shear flow at $\dot{\gamma} = 10\,s^{-1}$. The shear flow experiments were carried out at 210 C

have resulted from the break-up of the dispersed PS phase during the compounding in the twin-screw extruder. It is of interest to observe the differences in size of the dispersed PS phase between this blend and the 90/10 PMMA/PS blend (compare *Figure 11a* and *Figure 10a*). (2) When a specimen was subjected to shear flow in the cone-and-plate rheometer at a shear rate as low as $0.1\,s^{-1}$, the PS droplets were elongated along the flow direction, showing evidence that break-up occurred inside the gap between the cone and the plate (see *Figure 11b*). (3) When a specimen was subjected to shear flow in the capillary rheometer at $\dot{\gamma} = 10\,s^{-1}$, very long streaks of the dispersed PS phase are seen along the flow direction (see *Figure 11c*). It is of interest to observe that the areas of some dispersed PS phase in *Figure 11c* are much larger than those in *Figure 11b*. This appears to suggest that, during the flow inside the capillary, coalescence between the elongated PS droplets, flowing side by side, might have taken place. (4) When the shear rate was increased further to $100\,s^{-1}$, long fibril-like dispersed PS phase is observed along the flow direction.

Figure 12 gives micrographs for the 50/50 PMMA/PS blend before and after being subjected to shear flow at 210°C. The following observations are worth noting in *Figure 12*. (1) The phase morphology of this blend (see *Figure 12a*), as obtained from the extrusion in a twin-screw extruder, looks quite different from that of the other two blends considered above, namely 90/10 PMMA/PS and 70/30 PMMA/PS blends. It is of interest to observe that small amounts of the PS phase are occluded in the large domains of the PMMA phase, while the PS phase formed the continuous phase. (2) When a

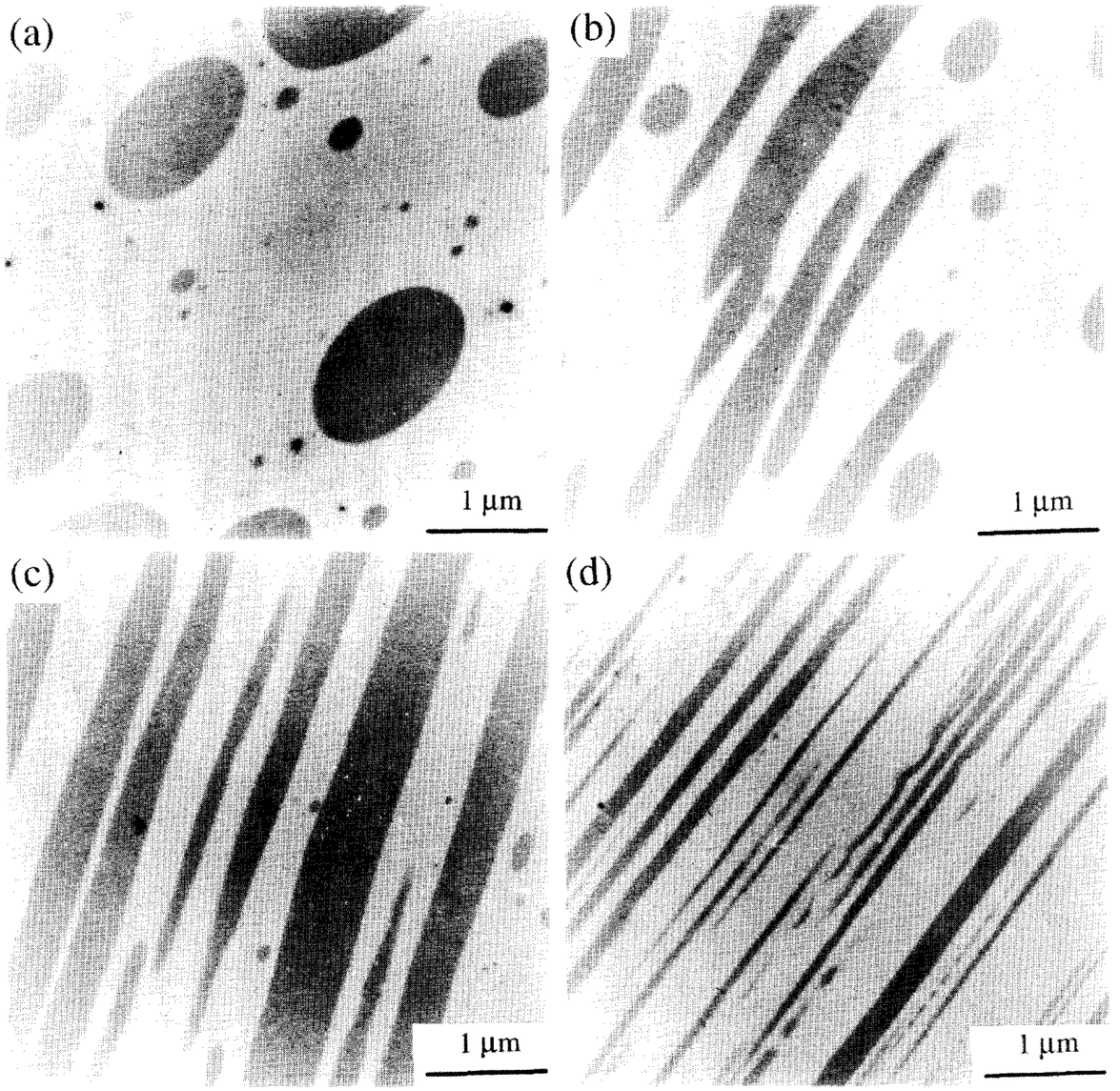

Figure 11 Micrographs for the 70/30 PMMA/PS blend, in which the dark area represents the PS phase and the white area represents the PMMA phase: (a) before being subjected to shear flow; (b) along the flow direction after being subjected to shear flow at $\dot{\gamma} = 0.1\,s^{-1}$; (c) along the flow direction after being subjected to shear flow at $\dot{\gamma} = 10\,s^{-1}$; (d) along the flow direction after being subjected to shear flow at $\dot{\gamma} = 100\,s^{-1}$. The shear flow experiments were carried out at 210°C

specimen was sheared in the cone-and-plate rheometer at $\dot{\gamma} = 1\,s^{-1}$, the cross-section of the specimen shows a very complex morphology (see *Figure 12b*) in that many PS droplets of smaller size are occluded in PMMA phase of much larger size. (3) When examining the phase morphology of the specimen along the flow direction (see *Figure 12c*), we observe clear evidence that coalescence took place during the flow inside the gap between the cone and the plate. (4) When a specimen was subjected to shear flow in the capillary rheometer at $\dot{\gamma} = 10\,s^{-1}$ (see *Figure 12d*), we observe a morphology having two almost co-continuous phases, strong evidence that very extensive coalescence took place during the flow inside the capillary.

Figure 13 gives micrographs for the 30/70 PMMA/PS blend before and after being subjected to shear flow at 210°C. The following observations are worth noting in *Figure 13*. (1) We now observe from *Figure 13a* that the PMMA phase forms droplets dispersed in the PS phase. In the particular PMMA/PS blend system investigated in this study, it appears that phase inversion takes place at an approximately equal blend ratio. In other words, the minor component forms the discrete phase and the major component forms the continuous phase. (2) When this blend was subjected to shear flow in the cone-and-plate rheometer at $\dot{\gamma} = 0.1\,s^{-1}$, little change in morphology is observed as compared to the morphology of the specimen before being subjected to shear flow (compare *Figure 13b* with *Figure 13a*). (3) However, when a specimen was subjected to shear flow in the capillary rheometer at $\dot{\gamma} = 10$ and $100\,s^{-1}$, we observe that the dispersed PMMA droplets were elongated considerably

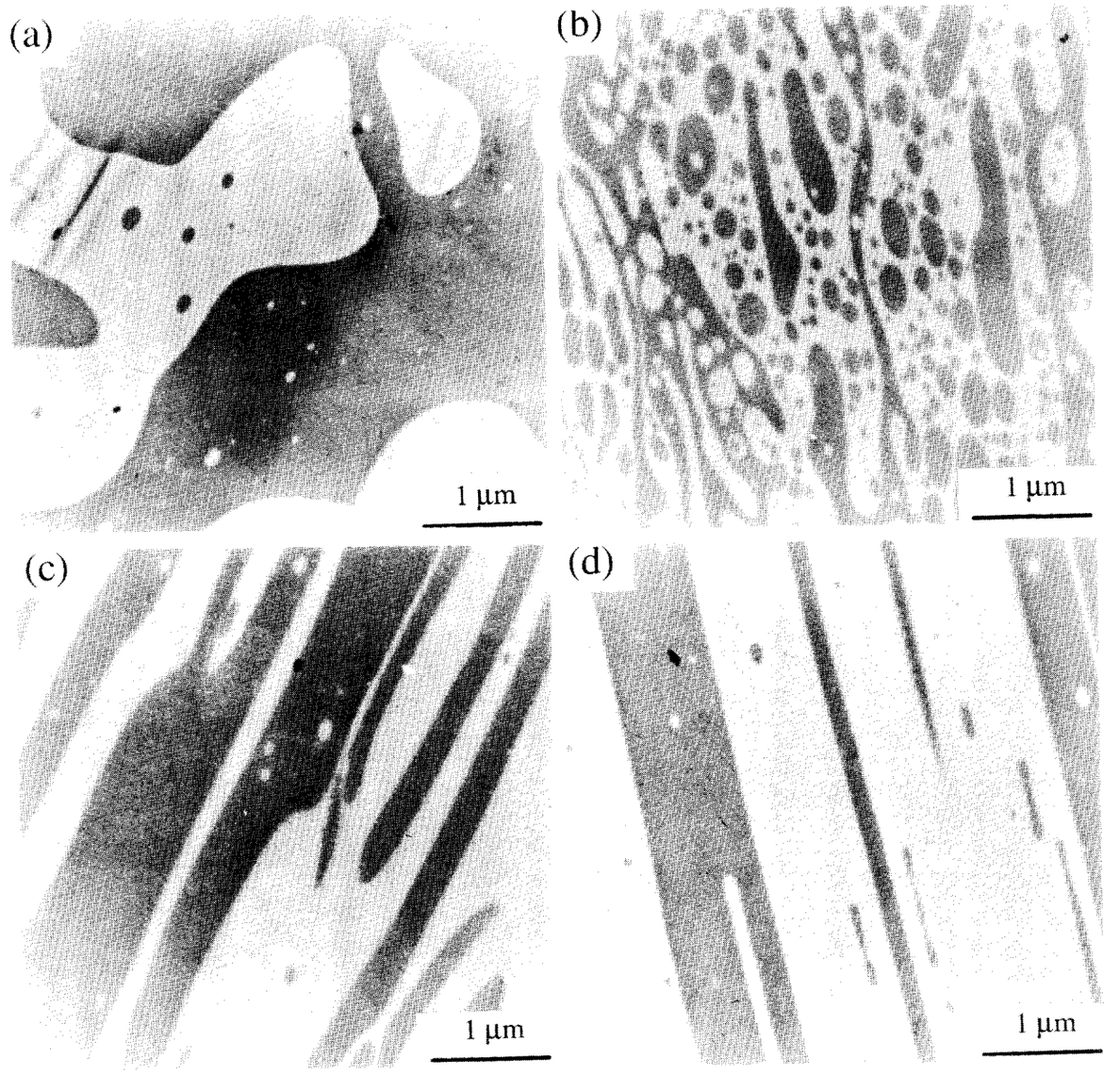

Figure 12 Micrographs for the 50/50 PMMA/PS blend, in which the dark area represents the PS phase and the white area represents the PMMA phase: (a) before being subjected to shear flow; (b) the cross-section of the specimen after being subjected to shear flow at $\dot{\gamma} = 1\,s^{-1}$; (c) along the flow direction after being subjected to shear flow at $\dot{\gamma} = 1\,s^{-1}$; (d) along the flow direction after being subjected to shear flow at $\dot{\gamma} = 10\,s^{-1}$. The shear flow experiments were carried out at 210 C

along the flow direction, very similar to the situations observed above for the 90/10 PMMA/PS and 70/30 PMMA/PS blends.

Oscillatory shear flow properties of PMMA/PS blends

Figure 14 gives the plots of log η *versus* log $\dot{\gamma}$ and log $|\eta^*|$ *versus* log ω for homopolymer PMMA at 210 and 230°C. Similar plots are given in *Figure 15* for the 50/50 PMMA/PS blend at 210 and 230°C. It can be seen in *Figures 14* and *15* that the Cox–Merz rule[21] holds for the homopolymer PMMA, but not for the 50/50 PMMA/PS blend. When considering the fact that the state of the dispersion in the 50/50 PMMA/PS blend in steady shear flow would be different from that in oscillatory shear flow, one should not be surprised to observed in *Figure 15* that the Cox–Merz rule does not hold for the 50/50 PMMA/PS blend. This observation would hold for other blend compositions in the PMMA/PS blend system and also for multiphase polymer systems in general.

Figure 16 gives plots of log G' *versus* log ω, and log G'' *versus* log ω for the homopolymer PMMA at 210, 220 and 230°C. It can be seen in *Figure 16* that values of G' and G'' decrease with increasing temperature. However, when the values of G' are plotted against the values of G'' on logarithmic coordinates, we obtain a correlation which is virtually independent of temperature, as given in *Figure 17* for homopolymers PS and PMMA at 210, 220 and 230°C. It should be mentioned that similar observations were made previously for other homopolymers[22–25]. As will be elaborated on below, plots of log G' *versus* log G'' are very useful in discussing the rheological behaviour of multicomponent and/or multiphase polymer systems[26].

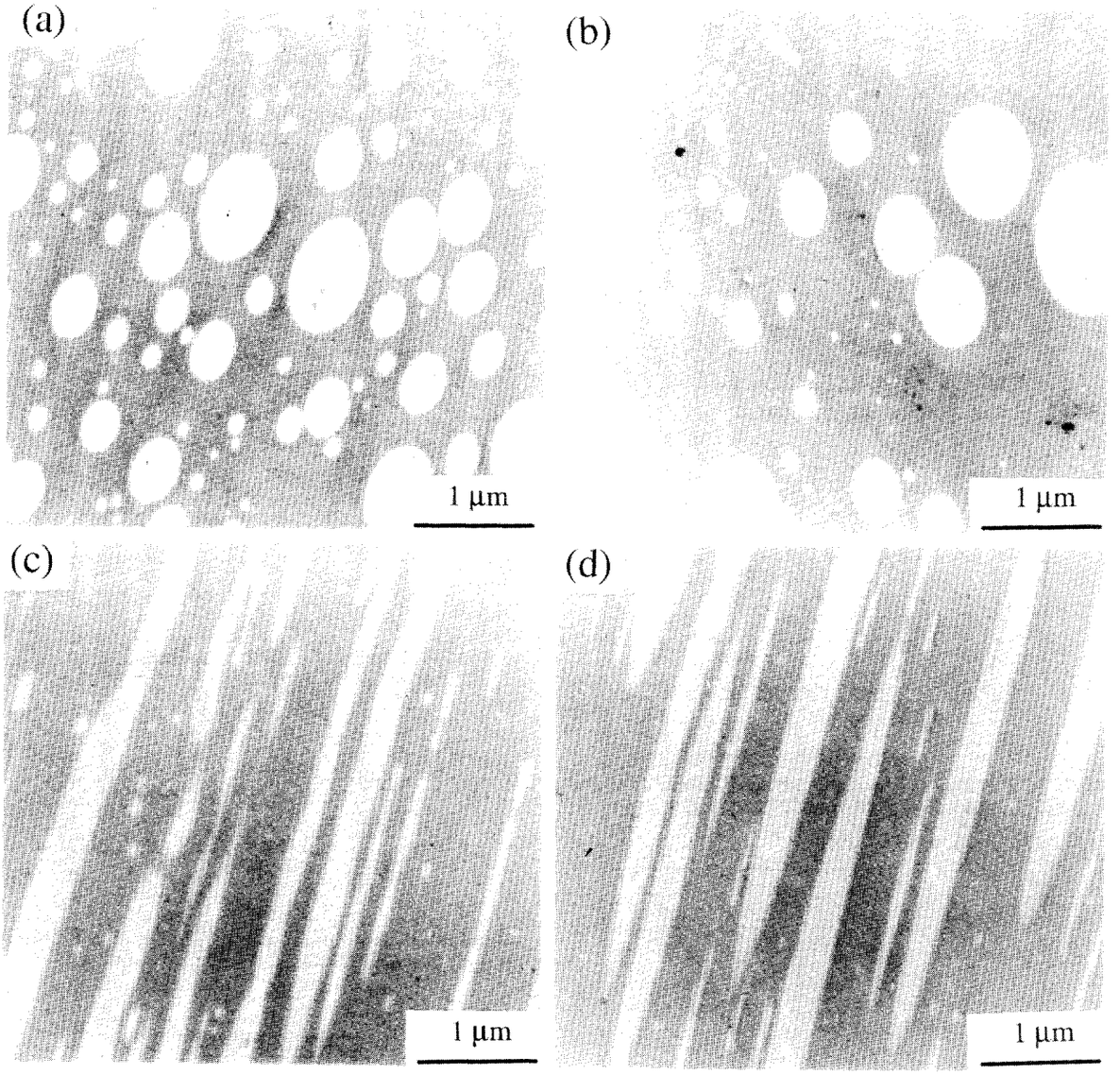

Figure 13 Micrographs for the 30/70 PMMA/PS blend, in which the dark area represents the PS phase and the white area represents the PMMA phase: (a) before being subjected to shear flow; (b) along the flow direction after being subjected to shear flow at $\dot{\gamma} = 0.1\ s^{-1}$; (c) in the flow direction after being subjected to shear flow at $\dot{\gamma} = 10\ s^{-1}$; (d) in the flow direction after being subjected to shear flow at $\dot{\gamma} = 100\ s^{-1}$. The shear flow experiments were carried out at 210°C

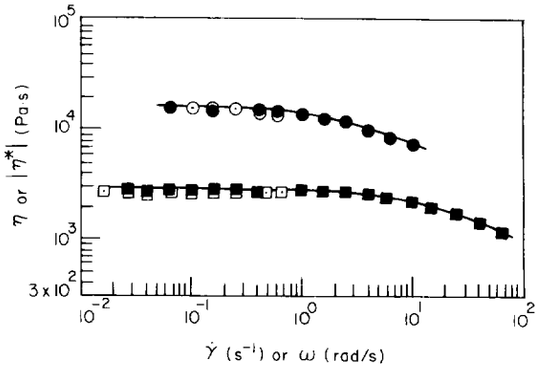

Figure 14 Plots of $\log \eta$ *versus* $\log \dot{\gamma}$ and $\log |\eta^*|$ *versus* $\log \omega$ for the homopolymer PMMA at 210°C (⊙, ●) and 230°C (□, ■), where open symbols denote η and filled symbols denote $|\eta^*|$

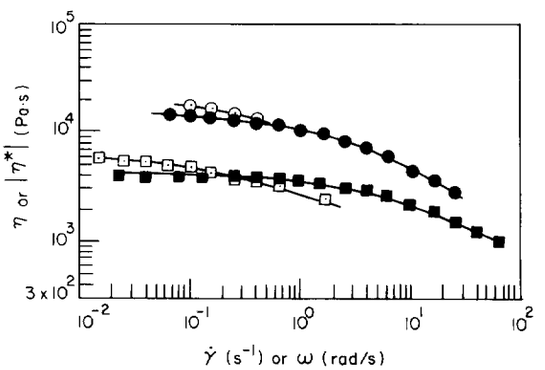

Figure 15 Plots of $\log \eta$ *versus* $\log \dot{\gamma}$ and $\log |\eta^*|$ *versus* $\log \omega$ for the 50/50 PMMA/PS blend at 210°C (⊙, ●) and 230°C (□, ■), where open symbols denote η and filled symbols denote $|\eta^*|$

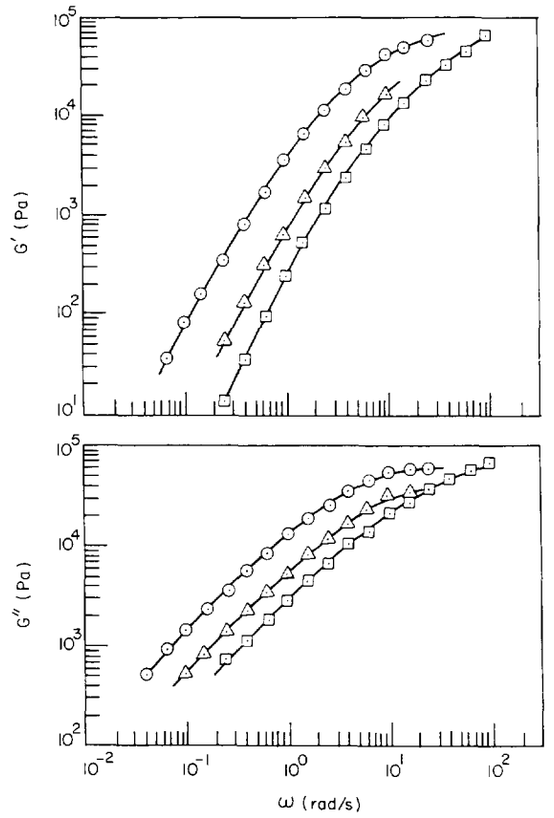

Figure 16 Plots of log G' *versus* log ω and log G'' *versus* log ω for homopolymer PMMA at (⊙) 210 C, (△) 220 C, (⊡) 230 C

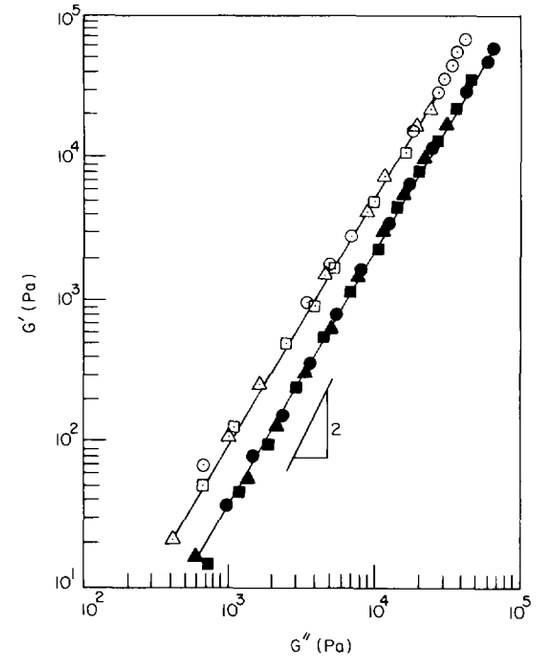

Figure 17 Plots of log G' *versus* log G'': homopolymer PS at (⊙) 210 C, (△) 220 C, (⊡) 230 C; homopolymer PMMA at (●) 210 C, (▲) 220 C, (■) 230 C

Plots of log G' *versus* log G'' are given in *Figure 18* for the 70/30 PMMA/PS blend at 210, 220 and 230°C, in *Figure 19* for the 50/50 PMMA/PS blend at 210, 220 and 230°C, and in *Figure 20* for the 30/70 PMMA/PS blend at 210, 220 and 230°C. The following observations are worth noting in *Figures 18–20*. (1) In contrast to the situation with homopolymers PS and PMMA (see *Figure 17*), plots of log G' *versus* log G'' for a PMMA/PS blend no longer have the slope of 2 in the terminal region. (2) The shape of log G' *versus* log G'' plots is different for each blend composition, apparently reflecting a different state of dispersion at each blend composition. As shown below, each of the PMMA/PS blends indeed has a different state of dispersion. At present, we are not able

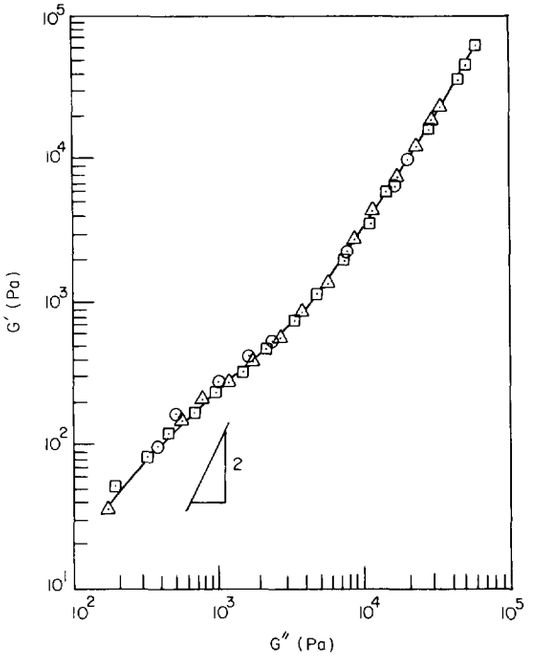

Figure 18 Plots of log G' *versus* log G'' for the 70/30 PMMA/PS blend at (⊙) 210 C, (△) 220 C, (⊡) 230 C

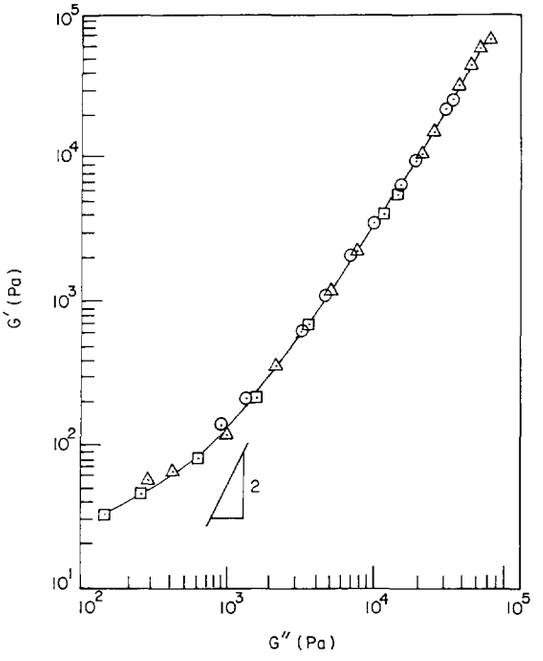

Figure 19 Plots of log G' *versus* log G'' for the 50/50 PMMA/PS blend at (⊙) 210 C, (△) 220 C, (⊡) 230 C

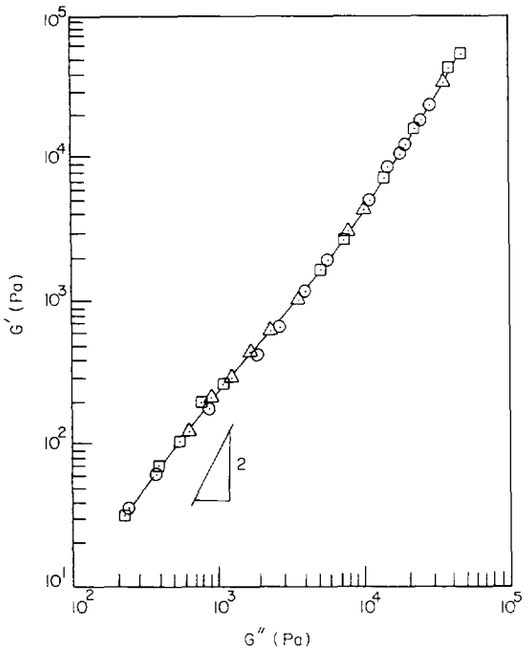

Figure 20 Plots of log G' *versus* log G'' for the 30/70 PMMA/PS blend at (○) 210°C, (△) 220°C, (□) 230°C

to correlate the shape of log G' *versus* log G'' plots to the state of dispersion in a PMMA/PS blend. Nevertheless, it can be stated that the shape of log G' *versus* log G'' plots for the PMMA/PS blend system varied with blend composition and thus with the morphological state of the blend.

It is of interest to note in *Figures 18–20* that plots of log G' *versus* log G'' for the PMMA/PS blends vary little with temperature between 210 and 230°C, in spite of the fact that they formed two phases (see *Figures 10–13*). This seems to suggest that the morphological state of the blend changed little with temperatures between 210 and 230°C. Since the critical temperature at which a PMMA/PS blend may form a single phase is expected to be exceedingly high as compared to the measurement temperatures employed, it would not be possible to reach this critical temperature by raising the measurement temperature without having thermal degradation. If there were significant morphological changes occurring in a PMMA/PS blend with increasing temperature, we would expect to observe temperature dependence of log G' *versus* log G'' plots. On the other hand, Han and co-workers[27–29] have reported that plots of log G' *versus* log G'' for a microphase-separated block copolymer exhibited temperature dependence until reaching a certain critical temperature at which the block copolymer became homogeneous. The difference observed in the temperature dependence of log G' *versus* log G'' plots between PMMA/PS blends and microphase-separated block copolymers comes from the fact that while the morphology of the PMMA/PS blends changed little in the temperature range from 210 to 230°C, in the microphase-separated block copolymers the extent of segmental miscibility between the two blocks increased with increasing temperature, eventually giving rise to a homogeneous phase at a critical temperature, which was within the temperature range of measurement (i.e. below the degradation temperature).

CONCLUDING REMARKS

In this paper we have presented experimental results, showing that plots of log η *versus* log σ for PMMA/PS blends obtained from a cone-and-plate rheometer do not overlap those obtained from a capillary rheometer. We attribute the experimental observation to differences in blend morphology, because the droplet deformation in the entrance region of a cylindrical die and subsequent recoil or break-up upon passing the entrance region can give rise to very complicated blend morphology in a non-uniform shear flow field (i.e. in a capillary rheometer). The interpretation of the rheological data offered in this paper may also be applicable to other multiphase polymer systems, such as microphase-separated block copolymers and thermotropic liquid-crystalline polymers (TLCPs).

We observed that in the PMMA/PS blends investigated in this study, the minor component formed the discrete phase and the major component formed the continuous phase. However, the 50/50 PMMA/PS blend produced a very complex, and yet intriguing, phase morphology which was not observed at other blend compositions. The micrographs presented in this paper show clearly that a better understanding of the rheological behaviour of a two-phase blend must be based on the state of dispersion of the material while flowing in a rheometer. Owing to the fact that the morpholgoical state of a two-phase polymer blend depends strongly on the intensity of the deformation applied, there is no reason why one should expect that the rheological properties measured from a cone-and-plate rheometer should coincide with those measured from a capillary rheometer. This leads us to conclude that rheological behaviour of two-phase polymer blends (also, multiphase polymer systems in general) is expected to be dependent upon the geometry of the rheometer employed.

Recently, Frayer and Huspeni[30] reported that the shear viscosities of TLCPs (Amoco Performance Products, XYDAR 2145 and XYDAR 2151) obtained from a slit die were different from those obtained from a capillary die. Moreover, they obtained negative values of the Bagley end correction for the TLCPs. In view of the fact that negative values of the Bagley end correction have no rheological significance, such an experimental observation reinforces our contention, presented above, that the use of equation (3) for the calculation of shear stress for multiphase polymer systems in a cylindrical die is of no rheological significance. Under such circumstances, the use of equation (2) is most desirable; this requires measurements of wall normal stresses along the die axis in the fully developed region[1–8]. In view of the fact that TLCPs in general have very complex morphologies in a liquid-crystalline state, the experimental observation made by Frayer and Huspeni reinforces our view that the rheological properties of morphologically complex polymeric liquids may be influenced greatly by the flow geometries employed, because the state of dispersion would be different in different types of flow geometry.

Thus, we conclude that one should not expect to observe an agreement in the rheological properties of multiphase polymer systems (e.g. two-phase polymer blends, microphase-separated block copolymers, and liquid-crystalline polymers), which were obtained from rheometers having different flow geometries.

REFERENCES

1 Han, C. D. 'Rheology in Polymer Processing', Academic Press, New York, 1976, Ch. 7
2 Han, C. D. 'Multiphase Flow in Polymer Processing', Academic Press, New York, 1981, Ch. 4
3 Han, C. D. and Yu, T. C. *J. Appl. Polym. Sci.* 1971, **15**, 1163
4 Han, C. D. *J. Appl. Polym. Sci.* 1971, **15**, 2591
5 Han, C. D. and Yu, T. C. *Polym. Eng. Sci.* 1972, **12**, 81
6 Han, C. D. and Kim, Y. W. *Trans. Soc. Rheol.* 1975, **19**, 245
7 Han, C. D. and Kim, Y. W. *J. Appl. Polym. Sci.* 1975, **19**, 2831
8 Kim, Y. W. and Han, C. D. *J. Appl. Polym. Sci.* 1976, **20**, 2905
9 Van Oene, H. *J. Colloid Interface Sci.* 1972, **40**, 448
10 Ablazova, T. I., Tsenbrenko, M. B., Yudin, A. B. V., Vinogradov, G. V. and Yarlykov, B. V. *J. Appl. Polym. Sci.* 1975, **19**, 1781
11 Lyngaae-Jorgansen, J., Andersen, F. E. and Alle, N. in 'Polymer Alloys III' (Eds. D. Klempner and K. C. Frisch), Plenum Press, New York, 1983, p. 105
12 Min, K., White, J. L. and Fellers, J. F. *J. Appl. Polym. Sci.* 1984, **29**, 2117
13 Han, C. D. 'Rheology in Polymer Processing', Academic Press, New York, 1976, Ch. 5
14 Han, C. D. and Charles, M. *AIChE J.* 1970, **16**, 499
15 Chin, H. B. and Han, C. D. *J. Rheol.* 1979, **23**, 557
16 Chin, H. B. and Han, C. D. *J. Rheol.* 1980, **24**, 1
17 Brizitsky, V. I., Vinogradov, G. V., Isayev, A. I. and Podolsky, Y. Y. *J. Appl. Polym. Sci.* 1978, **22**, 751
18 Yoo, H. J. and Han, C. D. *J. Rheol.* 1981, **25**, 115
19 Han, C. D. 'Multiphase Flow in Polymer Processing', Academic Press, New York, 1981, Ch. 5
20 Han, J. H., Feng, D., Choi-Feng, C. and Han, C. D. *Polymer* 1995, **36**, 155
21 Cox, W. P. and Merz, E. H. *J. Polym. Sci.* 1958, **28**, 619
22 Han, C. D. and Lem, K. W. *Polym. Eng. Rev.* 1983, **2**, 135
23 Chuang, H. K. and Han, C. D. *J. Appl. Polym. Sci.* 1984, **29**, 2205
24 Han, C. D. and Jhon, M. S. *J. Appl. Polym. Sci.* 1986, **32**, 3809
25 Han, C. D. *J. Appl. Polym. Sci.* 1988, **37**, 167
26 Han, C. D. and Kim, J. K. *Polymer* 1993, **34**, 2533
27 Han, C. D. and Kim, J. *J. Polym. Sci., Part B: Polym. Phys.* 1987, **25**, 1741
28 Han, C. D., Kim, J. and Kim, J. K. *Macromolecules* 1989, **22**, 383
29 Han, C. D., Baek, D. M. and Kim, J. K. *Macromolecules* 1990, **23**, 561
30 Frayer, P. D. and Huspeni, P. J. *J. Rheol.* 1990, **34**, 1199